Dynamical Downscaling of Austral Summer Climate Forecasts over Southern Africa Using a Regional Coupled Model

J. V. RATNAM,* S. K. BEHERA,* S. B. RATNA,+ C. J. DE W. RAUTENBACH,# C. LENNARD,@ J.-J. LUO,& Y. MASUMOTO,** K. TAKAHASHI,++ AND T. YAMAGATA+

* *Research Institute for Global Change, and Application Laboratory, JAMSTEC, Yokohama, Japan*
+ *Application Laboratory, JAMSTEC, Yokohama, Japan*
# *Department of Geography, Geoinformatics and Meteorology, University of Pretoria, Pretoria, South Africa*
@ *Climate Systems Analysis Group, University of Cape Town, Cape Town, South Africa*
& *Centre for Australian Weather and Climate Research, Bureau of Meteorology, Melbourne, Australia*
** *Research Institute for Global Change, JAMSTEC, Yokohama, Japan*
++ *Application Laboratory, and Earth Simulator Center, JAMSTEC, Yokohama, Japan*

(Manuscript received 2 September 2012, in final form 12 February 2013)

ABSTRACT

The prediction skill of dynamical downscaling is evaluated for climate forecasts over southern Africa using the Advanced Research Weather Research and Forecasting (WRF) model. As a case study, forecasts for the December–February (DJF) season of 2011/12 are evaluated. Initial and boundary conditions for the WRF model were taken from the seasonal forecasts of the Scale Interaction Experiment-Frontier Research Center for Global Change (SINTEX-F) coupled general circulation model. In addition to sea surface temperature (SST) forecasts generated by nine-member ensemble forecasts of SINTEX-F, the WRF was also configured to use SST generated by a simple mixed layer Price–Weller–Pinkel ocean model coupled to the WRF model. Analysis of the ensemble mean shows that the uncoupled WRF model significantly increases the biases (errors) in precipitation forecasted by SINTEX-F. When coupled to a simple mixed layer ocean model, the WRF model improves the spatial distribution of precipitation over southern Africa through a better representation of the moisture fluxes. Precipitation anomalies forecasted by the coupled WRF are seen to be significantly correlated with the observed precipitation anomalies over South Africa, Zimbabwe, southern Madagascar, and parts of Zambia and Angola. This is in contrast to the SINTEX-F global model precipitation anomaly forecasts that are closer to observations only for parts of Zimbabwe and South Africa. Therefore, the dynamical downscaling with the coupled WRF adds value to the SINTEX-F precipitation forecasts over southern Africa. However, the WRF model yields positive biases (>2°C) in surface air temperature forecasts over the southern African landmass in both the coupled and uncoupled configurations because of biases in the net heat fluxes.

1. Introduction

The agro-based economy of southern Africa is affected by interannual variations in austral summer [December–February (DJF)] precipitation. These variations are mostly caused by the landmass surface properties and synoptic system characteristics that are, to a great extent, affected by variations in sea surface temperatures (SSTs) in the global and surrounding oceans (Hirst and Hastenrath 1983; Reason and Mulenga 1999; Behera and Yamagata 2001; Reason 2001; Rouault et al. 2003a; Reason et al. 2006). For example, variations in SSTs of the surrounding oceans influence moisture advection toward southern Africa, which eventually affects precipitation over southern Africa. The variations in the Pacific Ocean are also known to indirectly affect precipitation over southern Africa (Nicholson and Kim 1997; Cook 2001; Reason and Jagadeesha 2005; Fauchereau et al. 2009), though the teleconnection between these SSTs and southern African precipitation is still not well understood. The dependence of the seasonal precipitation over southern Africa on the SSTs gives hope that the seasonal climate of southern Africa is predictable. Many studies have already been carried out in efforts to forecast austral summer precipitation over southern Africa (Joubert and Hewitson 1997; Mason and Joubert

Corresponding author address: J. V. Ratnam, 3173-25 Showa-machi, Kanazawa-ku, Yokohama, Kanagawa 236-0001, Japan.
E-mail: jvratnam@jamstec.go.jp

DOI: 10.1175/JCLI-D-12-00645.1

1997; Landman et al. 2009) using SSTs as predictors in atmospheric general circulation models (AGCMs). Most of these studies have indicated that precipitation is often overestimated over southern Africa in standalone AGCM simulations. Poor spatial representation of the boundary SSTs over the surrounding oceans might also lead to noticeable biases of precipitation forecasts (Rouault et al. 2003b). Encouraging is a study by Landman and Beraki (2012) that suggested ocean–atmosphere coupled general circulation models might have improved skill in forecasting seasonal precipitation over southern Africa, which could further be improved when a multimodel forecast approach is considered.

To reduce precipitation uncertainties in the GCM forecasts and to improve the spatial representation of such forecasts, dynamical downscaling using regional climate models (RCMs) could be considered (e.g., Giorgi 1990). Many attempts have already been made to downscale summer precipitation over southern Africa (Joubert et al. 1999; Hansingo and Reason 2008; Tadross et al. 2006; Kgatuke et al. 2008; MacKellar et al. 2009; Landman et al. 2009, Crétat et al. 2011a,b; Sylla et al. 2012). However, simulated precipitation by RCMs is known to still have biases, mainly because of physical parameterizations, errors in the lateral boundary conditions (Giorgi and Mearns 1999), and the two-tier approach of specifying observed or forecasted SST as a boundary input to the RCMs.

The one-tier approach of using coupled regional models (e.g., Seo et al. 2007; Xie et al. 2007; Ratnam et al. 2009) has shown better performance relative to the conventional two-tier approach. For example, Ratnam et al. (2012) have demonstrated that by coupling a simple mixed layer ocean model to the Advanced Research Weather Research and Forecasting (WRF) model (ARW; Skamarock et al. 2005) improved austral summer precipitation could be obtained over southern Africa. However, the WRF regional model in Ratnam et al. (2012) was driven by the National Centers for Environmental Prediction–National Center for Atmospheric Research (NCEP–NCAR) reanalysis data. In this framework, the downscaling skill represents the upper limit of regional predictability with near-perfect observed boundary conditions. It is of practical importance/use to examine how much regional skill we may gain with GCM forecasted boundary conditions. In this study, we use a similar approach of one-tier downscaling, but we downscale the seasonal forecasts of a global-coupled Scale Interaction Experiment-Frontier Research Center for Global Change (SINTEX-F; Luo et al. 2005) GCM. The WRF regional model is coupled to a simple mixed layer ocean model, the Price–Weller–Pinkel (PWP) model, based on Price et al. (1986), with a little higher complexity than that used in Ratnam et al. (2012). The aim of our study is twofold: 1) to see if the WRF model with specified SINTEX-F forecasted SST (WRFSSST) can reproduce the climate of southern Africa during the austral summer months of DJF 2011/12 and 2) to see if the WRF with the mixed layer ocean model (WRFPWP) could improve on the forecasts of WRFSSST.

2. Model and methodology

In this study, WRF-ARW, version 3.3 (Skamarock et al. 2005), is used for the dynamical downscaling of the GCM seasonal forecast over southern Africa. A horizontal resolution of 30 km covering the area 45°–4°S and 0.5°–60°E with 23 vertical levels was chosen for the study. The physics packages used in this study include the Rapid Radiative Transfer Model (RRTM) for the longwave radiation (Mlawer et al. 1997), a simple cloud-interactive shortwave radiation scheme (Dudhia 1989), the Kain–Fritsch cumulus parameterization scheme (Kain 2004), the Yonsei University (YSU) planetary boundary layer scheme (Hong et al. 2006), the Noah land surface scheme (Chen and Dudhia 2001) with 24 U.S. Geological Survey (USGS) land surface categories, and the WRF single-moment three-class (WSM3) microphysics scheme (Hong et al. 2004). The choice of these physics packages is consistent with that of Crétat et al. (2011b) and Ratnam et al. (2012) for the simulation of climate of southern Africa.

For the downscaling experiment in this case study, an ensemble of nine WRF model forecasts were generated using the initial and boundary conditions from the nine members of the SINTEX-F coupled global model 3-month lead forecasts. The atmospheric component (ECHAM4.6; Roeckner et al. 1996) of SINTEX-F has a resolution of 1.1° (T106) with 19 vertical levels. Its oceanic component [Océan Parallélisé (OPA) 8; Madec et al. 1998] has a relatively coarse resolution of a 2° Mercator horizontal mesh but with an equatorial intensification up to 0.5° in meridional direction with 31 levels in vertical. Heat, water, and momentum fluxes across the air–sea interface are exchanged every 2 h without any corrections using a standardized Ocean Atmosphere Sea Ice Soil, version 2.0 (OASIS2), coupler. The SINTEX-F has been applied to various climate studies and proved to have good performance in simulating and predicting the tropical climate such as ENSO and Indian Ocean dipole (IOD). As a case study, forecasts for DJF 2011/12 with November 2011 initial conditions were considered. The nine ensemble members of the SINTEX-F forecast used in this study are generated by perturbing both the model-coupling physics and initial conditions with different

SST-nudging coefficients as described in Luo et al. (2007, 2008).

As was shown in Ratnam et al. (2012), the WRF model coupled to a simple mixed layer ocean model improved the simulation of the austral summer precipitation over southern Africa, in contrast to simulation with prescribed SSTs. The results of Ratnam et al. (2012) were based on the model runs with the reanalysis data as boundary conditions. In the present study, we see if such improvements can be seen using boundary conditions from the SINTEX-F coupled model forecasts. The one-dimensional PWP mixed layer ocean model based on Price et al. (1986) is coupled to the WRF model to study the effect of air–sea interactions on the seasonal forecast of the austral summer season of 2011/12 generated by the WRF model. The WRF and PWP models are coupled to have two-way interactions between them. The PWP model is driven by surface heat fluxes and wind stress from the WRF model, and the sea surface temperatures simulated by the PWP are passed back to WRF at each grid point.

Surface temperatures simulated by the PWP model depend on the simulated mixed layer depth. In the PWP model, the mixed layer depth is calculated based on the vertical heat and momentum fluxes at a given point to determine the deepening or shallowing of the mixed layer, irrespective of horizontal or vertical advective processes. Vertical mixing in the PWP model takes place in such a way as to satisfy the conditions for static stability, mixed layer stability (indicated by the bulk Richardson number Ri_b), and shear flow instability (indicated by the gradient Richardson number Ri_g). As surface fluxes are provided to the PWP model at each time step, vertical mixing occurs until all three conditions are met throughout the profile. As the model runs, solar radiation is absorbed and surface heat loss is removed from the uppermost meter of the water column at each time step. Densities are then computed and mixed to achieve static stability. Next, wind stress is absorbed and a value of Ri_b is computed and compared with the critical value of 0.65. Entrainment of denser water from below the mixed layer takes place as necessary to achieve static stability. Price et al. (1986) also include the shear flow stability requirement to account for the fact that their observations indicate a smooth transition layer below the mixed layer, as opposed to the sharp jump assumed by other models, and because shear instability is likely at levels of strong stratification. The Ri_g is calculated only within this transition layer and mixing takes place until it is above the critical value of 0.25 throughout this region. This has the effect of smoothing out the transition from the mixed layer to the region below. In this study, the PWP model was run on a vertical grid of 1-m resolution with 300 vertical levels within the top 300-m depth. The high resolution in the vertical helps to improve the simulation of a diurnal cycle. The initial vertical profiles of temperature and salinity are climatological ones derived from the NCEP Global Ocean Data Assimilation System (GODAS). Heat fluxes and wind stress input was provided to the PWP model at every step of the WRF model and at the same time intervals the WRF model was updated with PWP model simulated SST.

In both the experiments, with SST from either the SINTEX-F forecast (i.e., WRFSSST) or the mixed layer ocean model (i.e., WRFPWP), respective models were integrated for the study period using the initial and 6-hourly boundary conditions provided by the SINTEX-F coupled model. The 6-hourly SST forecasted by SINTEX-F was used as the lower boundary condition for the WRFSSST experiment. The models were initialized on 1 November 2011 and integrated until 29 February 2012.

The model forecasted precipitation during DJF 2011/12 is compared with the Tropical Rainfall Measuring Mission (TRMM) estimated monthly precipitation [3B43, version 7 (3B43V7); Huffman et al. 2007]. In addition, the long-term climatology and precipitation anomalies are compared with the Climate Prediction Center (CPC) estimated Climate Anomaly Monitoring System (CAMS) and outgoing longwave radiation (OLR) precipitation index (OPI) (CAMS–OPI), version 0208, precipitation anomalies (Janowiak and Xie 1999), because of the limited time period of the TRMM estimates. The SSTs during DJF 2011/12 are compared with the National Oceanic and Atmospheric Administration (NOAA) optimum interpolation SST, version 2 (OISST2; Reynolds et al. 2002), estimates. The large-scale atmospheric fields simulated by the models are compared with the European Centre for Medium-Range Weather Forecasts (ECMWF) Interim Re-Analysis (ERA-Interim; Dee et al. 2011) data. The land surface temperatures forecasted by the models are compared with the CPC NCEP Global Historical Climatology Network, version 2, and the CAMS (GHCN–CAMS) (Fan and Van den Dool 2008) estimates. The significance of the model simulated forecasts and their biases are calculated to validate all of the members of the ensemble using a Student's t test. Significance shows the agreement between ensemble members. The ensemble mean of the bias/anomalies is based on the bias/anomalies estimated from each member of the ensemble. The model bias (error) refers to model forecasts minus observation differences and anomaly refers to the departure from the mean throughout the text.

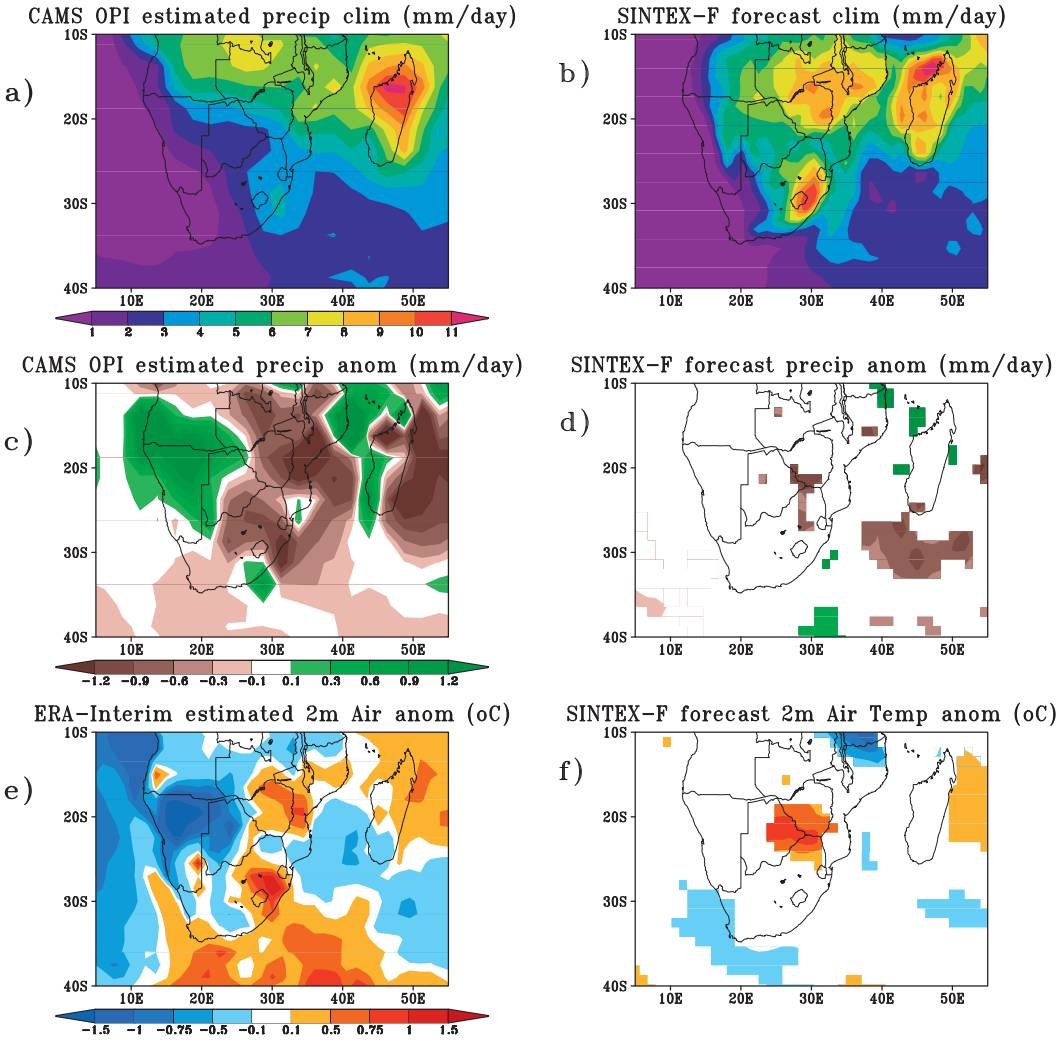

FIG. 1. (a) The CAMS–OPI estimated DJF precipitation climatology (mm day^{-1}; mean of DJF 1983/84–DJF 2005/06). (b) SINTEX-F forecasted precipitation DJF climatology (mm day^{-1}) based on DJF 1983/84–DJF 2005/06. (c) CAMS–OPI estimated DJF 2011/12 precipitation anomalies (mm day^{-1}). (d) Significant (at 90% using a Student's *t* test) SINTEX-F model nine-member mean forecasted precipitation anomalies. (e) ERA-Interim estimated 2-m air temperature anomalies during DJF 2011/12. (f) As in (d), but for the significant SINTEX-F model forecasted 2-m air temperature anomalies.

3. Results

a. SINTEX-F forecasted climatology and DJF 2011/12 anomalies

The CAMS–OPI estimated precipitation climatology (mean of DJF 1983/84–DJF 2006/07) (Fig. 1a), shows a precipitation peak over Madagascar, Mozambique, Zambia, and Angola, along the Intertropical Convergence Zone (ITCZ) with a secondary peak over South Africa. The nine-member ensemble-mean SINTEX-F forecasted DJF precipitation climatology (mean of DJF 1983/84–DJF 2006/07) (Fig. 1b) shows a south- and eastward shift in precipitation peak over southern Africa relative to the CAMS–OPI estimated precipitation. The maxima in the SINTEX-F forecasted precipitation climatology are seen over Mozambique, Zimbabwe, and Zambia. Also, the precipitation over South Africa is of higher intensity than the CAMS–OPI estimated precipitation. During DJF 2011/12, the observed anomalies show that, except for parts over Angola, Namibia, and Mozambique, most parts of southern Africa received less than normal precipitation (Fig. 1c). The spatial distribution of the ensemble mean of the SINTEX-F forecasted anomalies for DJF 2011/12, however, shows significant precipitation anomalies only over parts of South Africa, Zimbabwe, and Botswana (Fig. 1d). The 2-m air temperature anomaly estimated from ERA-Interim (with respect to ERA-Interim 2-m air temperature

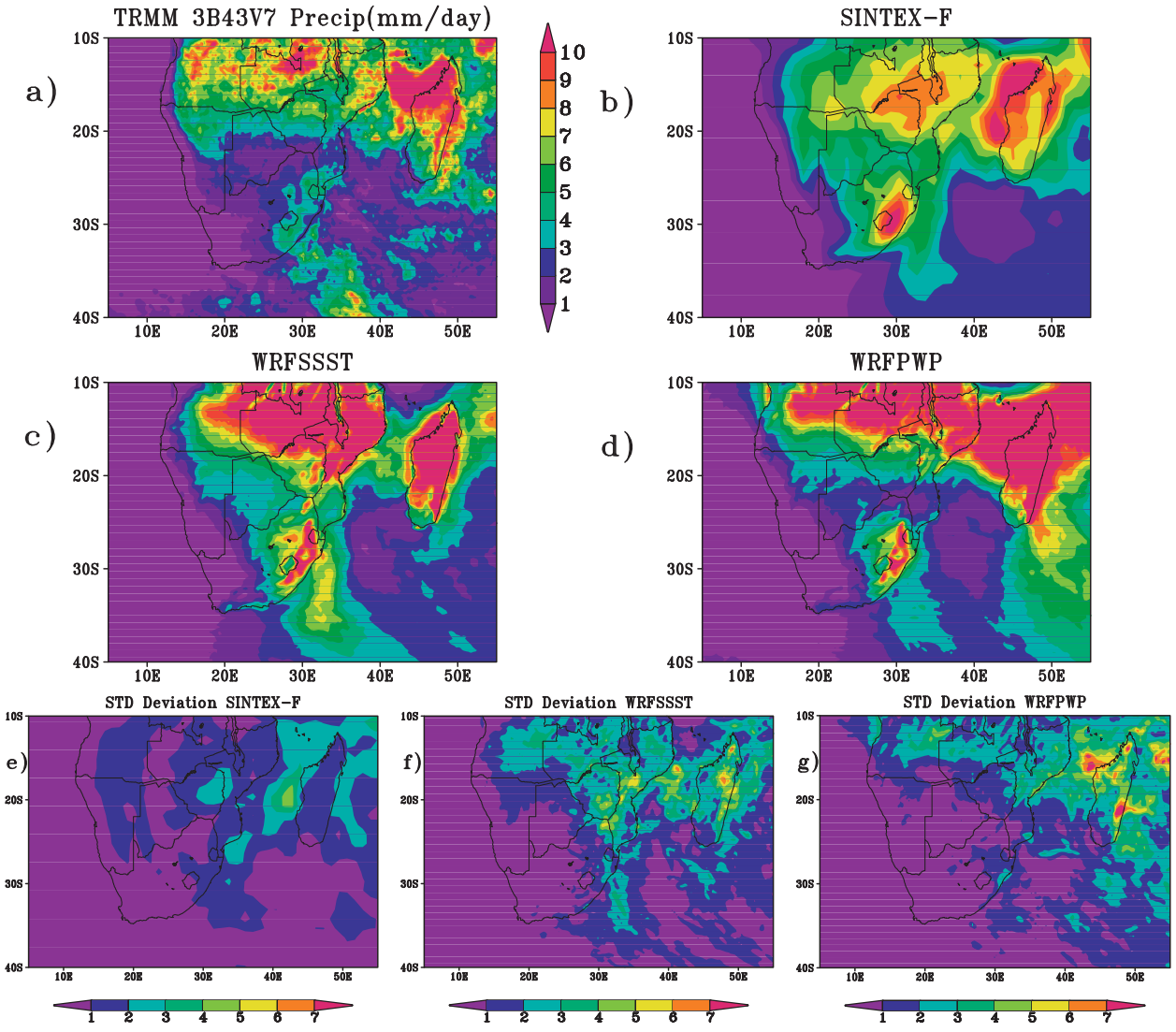

FIG. 2. (a) The TRMM 3B43V7 estimated precipitation during DJF 2011/12 (mm day^{-1}). (b) SINTEX-F forecasted ensemble-mean significant precipitation (mm day^{-1}) for DJF 2011/12. (c) WRFSSST forecasted ensemble-mean significant precipitation (mm day^{-1}) and (d) WRFPWP forecasted ensemble-mean significant precipitation (mm day^{-1}) during DJF 2011/12. (e) Std dev of SINTEX-F forecasted DJF 2011/12 precipitation with respect to its ensemble mean. (f) As in (e), but for the WRFSSST forecasted precipitation. (g) As in (e), but for the WRFPWP forecasted precipitation. Precipitation in (b)–(d) is significant at 90% using a Student's *t* test.

climatology; DJF 1983/84–DJF 2006/07) during DJF 2011/12 (Fig. 1e) shows negative anomalies over most parts of southern Africa, with the exception of Zimbabwe and part of South Africa and Mozambique. The SINTEX-F forecasted significant 2-m air temperature anomalies for DJF 2011/12 (Fig. 1f) show positive values over Zimbabwe, though higher in magnitude.

b. Spatial distribution of forecasted precipitation and skill

Spatial distribution of the TRMM estimated precipitation during DJF 2011/12 (Fig. 2a) shows high precipitation (>6 mm day^{-1}) to be confined to Angola, Zambia, Mozambique, and Madagascar with moderate precipitation (3–6 mm day^{-1}) over Lesotho and eastern parts of South Africa. A high precipitation region is also evident along the South Indian Ocean convergence zone (Cook 2000, 2001) extending from the tropical to subtropical latitudes through South Africa (Fig. 2a). However, the rainband linking the tropical precipitation with subtropical precipitation is weak (Fig. 2a) during DJF 2011/12. The ensemble-mean SINTEX-F forecasted precipitation during DJF 2011/12 (Fig. 2b), similar to its climatological precipitation (Fig. 1b), shows significant

high precipitation throughout southern Africa with peaks in precipitation ($>8\,\mathrm{mm\,day^{-1}}$) over parts of Mozambique, Zimbabwe, and South Africa. The SINTEX-F forecast also shows high precipitation over the South Indian Ocean to the east of the southern Africa landmass. The ensemble mean of the WRF model, driven by the SINTEX-F atmospheric boundary conditions and SINTEX-F forecasted SST (WRFSSST) (Fig. 2c), forecasts higher precipitation over the entire southern Africa similar to SINTEX-F forecasts. Interestingly, the ensemble mean of the WRF model coupled to the PWP mixed layer ocean model (Fig. 2d) shows noticeable improvement in the forecasted precipitation over parts of Mozambique, Zimbabwe, and Botswana relative to the WRFSSST forecast (Fig. 2c), though the precipitation is higher over the tropical South Indian Ocean than in both the WRFSSST forecast and TRMM estimates. The standard deviation of the SINTEX-F forecasted precipitation during DJF 2011/12 with respect to its ensemble mean (Fig. 2e) shows values between 1 and $2\,\mathrm{mm\,day^{-1}}$ over the southern Africa landmass. The standard deviation of the forecasted precipitation within the WRFSSST members (Fig. 2f) is higher than SINTEX-F, with values between 2 and $3\,\mathrm{mm\,day^{-1}}$ over tropical regions of southern Africa and with values from 5 to $6\,\mathrm{mm\,day^{-1}}$ over parts of Mozambique. The WRFPWP members (Fig. 2g) show smaller standard deviations in the forecasted precipitation than WRFSSST members, showing that coupling to a simple mixed layer ocean model increases the forecast accuracy relative to forecasts with SST specified to the WRF model.

To get an estimate of the precipitation bias, the spatial distribution of the biases in the precipitation forecast is shown in Fig. 3. The ensemble-mean SINTEX-F biases in the forecasted precipitation with respect to TRMM estimates (Fig. 3a) shows significant negative biases of more than $3\,\mathrm{mm\,day^{-1}}$ over Angola and Zambia, the regions of high precipitation during DJF 2011/12, and significant positive biases of more than $3\,\mathrm{mm\,day^{-1}}$ occur over most of the other regions of southern Africa. The ensemble-mean WRFSSST forecast (Fig. 3b) shows significant positive biases of more than $3\,\mathrm{mm\,day^{-1}}$ over most parts of southern Africa, except for some parts over Angola and Namibia, with respect to the TRMM estimates. The WRFPWP forecasted (Fig. 3c) ensemble-mean bias shows improvement in the forecasted precipitation over Mozambique, Angola, and parts of Zambia and Zimbabwe relative to the biases in the precipitation forecasted by WRFSSST. However, the WRFPWP forecast also shows a significant positive bias of greater than $3\,\mathrm{mm\,day^{-1}}$ for parts of Zambia, Angola, and Mozambique. The precipitation bias in the WRFPWP forecasts over the tropical South Indian Ocean is higher than that of WRFSSST. The region of negative biases in precipitation in the WRFPWP forecast (Fig. 3c) over the southern Africa landmass is similar to the region forecasted by WRFSSST (Fig. 3b). Comparing the precipitation forecasted by WRFPWP with the precipitation forecasted by WRFSSST (Fig. 3d), it becomes evident that the WRF model coupled to the PWP mixed layer ocean model reduces the positive bias over Mozambique, Zimbabwe, and parts of Zambia and South Africa along the region of the ITCZ, though there is a substantial increase in precipitation over the South Indian Ocean to the east of Madagascar and over the tropical regions (Fig. 3d). The reduction of biases over the southern Africa landmass in the WRFPWP forecast further confirms the finding of Ratnam et al. (2012) that the inclusion of air–sea interaction in neighboring oceans could improve the spatial distribution of the precipitation over southern Africa.

Because of the uncertainties present in the observations over southern Africa (Sylla et al. 2013; Nikulin et al. 2012), the WRF model forecasts are also compared with precipitation estimates from the CPC Famine Early Warning System Network (FEWS NET) Africa Rainfall Estimation Algorithm, version 2 (RFEv2) (Figs. 3e,f). Precipitation biases of WRFSSST and WRFPWP forecasts show large differences over Angola and Namibia with respect to TRMM and CPC FEWS NET RFEv2. The negative bias over Angola and Namibia with respect to CPC RFEv2 (Figs. 3e,f) is smaller in magnitude than TRMM (Figs. 3b,c) estimates over the region. The improvement in the precipitation biases over Mozambique, Zimbabwe, and parts of Zambia and South Africa seen in the WRFPWP forecast (Fig. 3c) is also seen in the biases with respect to CPC RFEv2, showing the robustness of the improvement over those regions from coupling.

To get a quantitative estimate of the improvements in the WRF forecasts coupled to a simple mixed layer ocean model, spatial correlation (SC), root-mean-square error (RMSE), and bias-adjusted equitable threat score (Mesinger 2008) over the southern Africa landmass (31°–7°S, 11°–41°E), with masking out precipitation over the oceans and Madagascar, are calculated with respect to the TRMM estimates for all the members of the ensemble and are presented in Fig. 4. All the members of the SINTEX-F forecast have a lower spatial correlation relative to WRFSSST and WRFPWP (Fig. 4). From Fig. 4, it is clearly seen that most members of the WRFPWP ensemble show a higher spatial correlation of DJF 2011/12 precipitation forecasted with the TRMM estimates relative to the WRFSSST (Fig. 4) precipitation forecast. The ensemble mean of the WRFPWP forecast (0.81) also has higher correlation with TRMM estimates relative to the SINTEX-F (0.47) and WRFSSST

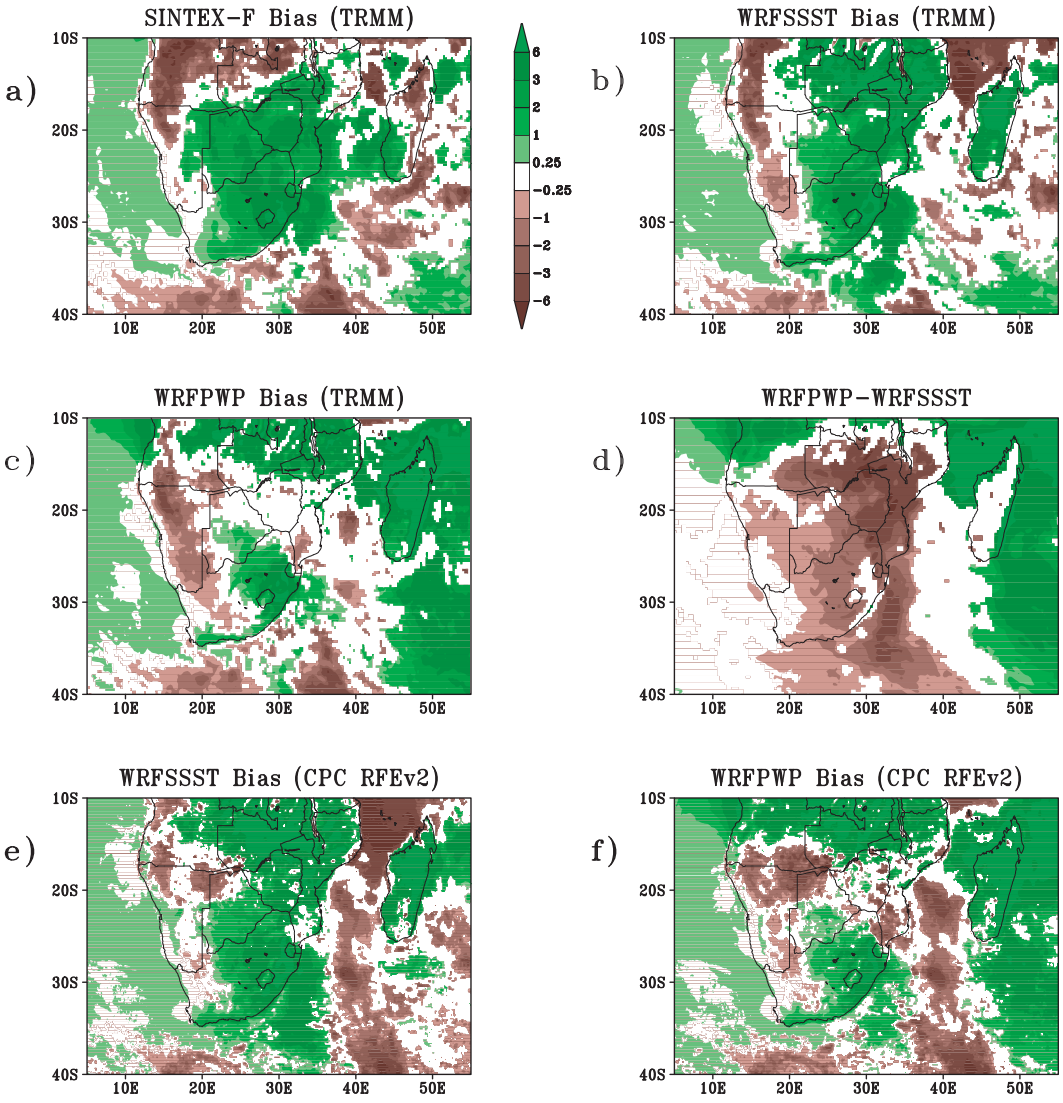

FIG. 3. (a) The ensemble-mean bias in the SINTEX-F forecasted precipitation (mm day^{-1}) with respect to TRMM estimates during DJF 2011/12. (b) As in (a), but for the bias in the WRFSSST forecast. (c) As in (a), but for the bias in the WRFPWP forecast. (d) Ensemble-mean difference between WRFPWP and WRFSST forecasted precipitation (mm day^{-1}) during DJF 2011/12. (e) Ensemble-mean bias in the WRFSSST forecasted precipitation (mm day^{-1}) with respect to CPC RFEv2 during DJF 2011/12. (f) As in (e), but for the mean bias in the WRFPWP forecasted precipitation (mm day^{-1}). Precipitation biases/differences are significant at 90% using a Student's *t* test.

(0.722) forecasts. All the members and the ensemble mean of the WRFPWP ensemble have a lower root-mean-square error than the WRFSSST members (Fig. 4). The ensemble-mean WRFPWP precipitation forecast (2.57) also has a smaller root-mean-square error than the WRFSSST forecast (3.34). The higher values of pattern correlation and lower values of root-mean-square error of WRFPWP forecasts clearly show the improvement in the WRF precipitation forecasts over southern Africa because of coupling to a simple mixed layer ocean model.

To further estimate the improvements in the WRF forecast skill because of coupling, we calculate the bias-adjusted equitable threat score (ETS) for all the members of the ensemble and the ensemble mean. Equitable threat score, as defined by Mesinger and Black (1992), is $(H - FO/N)/(F + O - H - FO/N)$, where FO/N is the number of points of random hits, N is the number of points in the verification domain, F is the number of points of predicted precipitation above a certain threshold, O is the number of points with observed precipitation above the threshold, and H is the number of hits.

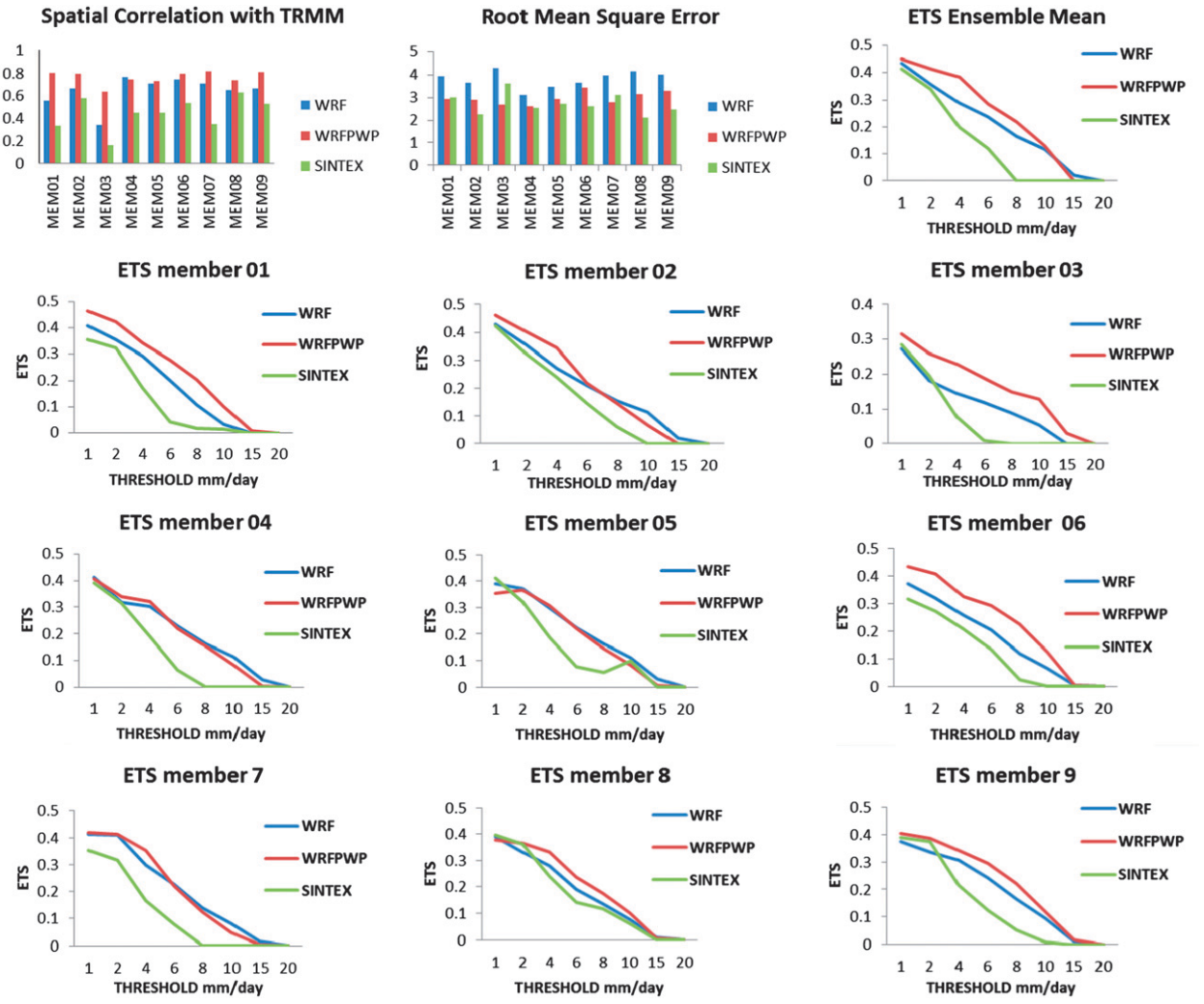

FIG. 4. The SC, RMSE, and bias-adjusted ETS of SINTEX-F, WRFSSST, and WRFPWP forecasts over the southern Africa landmass (31°–7°S, 11°–41°E) for DJF 2011/12 with respect to TRMM estimates.

The above formulation of equitable threat score was found to be strongly affected by bias F/O, with a higher bias giving higher scores. Bias-adjusted formulation of the above equation as defined in Mesinger (2008) replaces H with:

$$H_a = O - \left\{\frac{F-H}{\ln[O/(O-H)]}\right\} W\left[\left(\frac{O}{F-H}\right)\ln\left(\frac{O}{O-H}\right)\right],$$

where H_a is the adjusted H [Eq. (11) of Mesinger (2008)], F with O are from the ETS formulation, and W is the Lambert W function. The mean monthly precipitation forecasts of SINTEX-F, WRFSSST, and WRFPWP are considered in the calculation of ETS for DJF 2011/12. The ETS was calculated for threshold precipitation values of 2, 4, 6, 8, 10, 15, and 20 mm day^{-1}. The ensemble means of both WRFSST and WRFPWP forecasts show higher values of ETS than SINTEX-F forecasts (Fig. 4). The ETS score of the WRFPWP ensemble-mean forecast shows higher values up to a 10 mm day^{-1} threshold (Fig. 4) than the WRFSSST ensemble-mean forecast. Most of the members of the WRFPWP ensemble show higher scores relative to WRFSSST and SINTEX-F (Fig. 4), showing that the coupling of WRF to a simple mixed layer ocean model improved the forecasts of DJF 2011/12 over southern Africa.

c. *Vertically integrated moisture flux*

The analysis of the biases in precipitation forecasted by the different model configurations relative to the TRMM estimated precipitation shows that SINTEX-F and the WRFSSST model have significant positive biases over the southern Africa landmass. In contrast, the

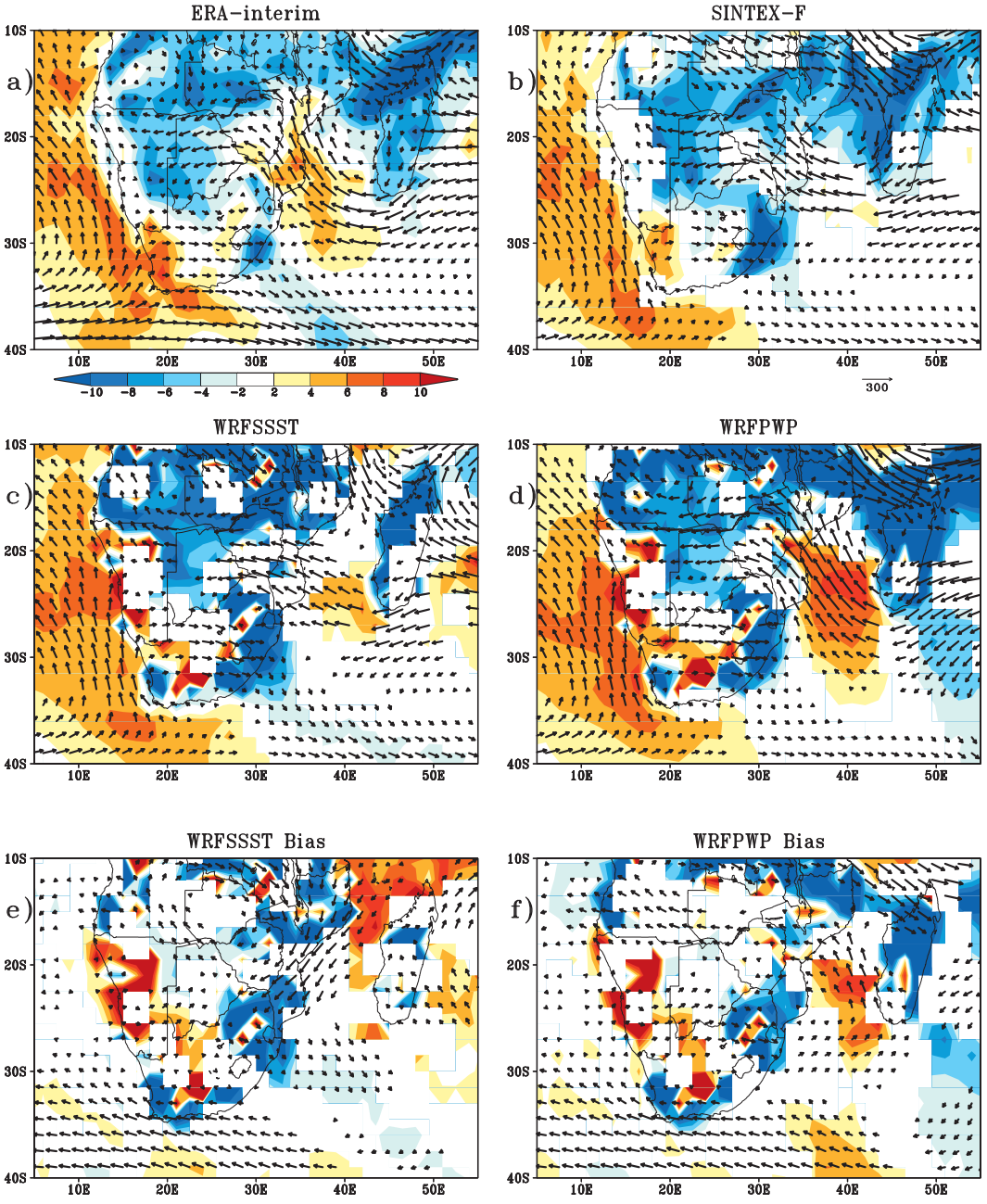

FIG. 5. (a) The ERA-Interim estimated vertically integrated moisture flux [vector; reference vector provided below panel (b)] and its divergence ($10^{-5}\,s^{-1}$; shaded) during DJF 2011/12. (b) Ensemble-mean SINTEX-F forecasted vertically integrated moisture flux ($kg\,m^{-1}\,s^{-1}$; vector) and divergence ($10^{-5}\,s^{-1}$; shaded) during DJF 2011/12. (c) As in (b), but for the forecast by WRFSSST. (d) As in (b), but for the forecast by WRFPWP. (e) As in (b), but for the WRFSSST bias with respect to ERA-Interim. (f) As in (e), but for the WRFPWP bias. The moisture flux and divergence in (b)–(f) are significant at 90% using a Student's *t* test.

WRFPWP model shows a reduction in the biases in the forecast relative to WRFSSST along the ITCZ.

To understand the causes of model biases in the spatial distribution of precipitation in the model forecasts, we analyzed the vertically integrated (from 1000 to 300 hPa) moisture fluxes and their divergence during DJF 2011/12. The ERA-Interim estimated moisture fluxes (Fig. 5a) show the moisture being transported into southern Africa during DJF 2011/12 from the southwestern Indian Ocean, along the ITCZ. The moisture is also transported

from the southeastern tropical Atlantic Ocean (Reason et al. 2006; Vigaud et al. 2007; Morioka et al. 2011) along the Angola low (Cook et al. 2004; Reason and Jagadeesha 2005), as seen over the Angola region (Fig. 5a). During DJF 2011/12, South Africa was mostly affected by the moisture fluxes from the southeastern subtropical Atlantic Ocean. However, over the northern part of South Africa the moisture fluxes from the southeastern subtropical Atlantic Ocean along with the fluxes from the southwestern Indian Ocean form an anticyclonic flow (Fig. 5a). The regions of vertically integrated moisture convergence are seen over Angola, Zambia, and northern Mozambique (Fig. 5a). These are also the regions of high precipitation (Fig. 2a) during DJF 2011/12. The regions of convergence are also seen over parts of South Africa, Botswana, and Namibia. The transport of moisture into southern Africa from the southwestern South Indian Ocean creates a region of moisture divergence over parts of Mozambique and over the oceanic regions to the east of southern Mozambique (Fig. 5a). The ensemble-mean SINTEX-F forecasted integrated moisture flux (Fig. 5b) shows significant enhanced moisture fluxes from the tropical regions into southern Africa, creating regions of moisture convergence over the regions of enhanced precipitation (Fig. 2b). The WRFSSST forecast (Fig. 5c), driven by the SINTEX-F forecasted boundaries, enhances the fluxes from both the tropical regions and from the southwestern Indian Ocean into the southern Africa landmass, creating a region of increased precipitation (Fig. 2c). The WRFPWP forecasted ensemble mean (Fig. 5d) shows larger transport of moisture into the tropical South Indian Ocean and also into the southern Africa landmass relative to WRFSSST forecast. The enhanced moisture flux into southern Africa along the ITCZ creates a region of enhanced precipitation over Zambia (Fig. 2d) in the WRFPWP forecast. However, both the WRFPWP and WRFSSST forecasts have stronger convergence of moisture fluxes over the southern Africa landmass relative to the ERA-Interim estimates, in agreement with the positive biases in precipitation over the landmass in both forecasts. Figure 5e shows a significant bias in the WRFSSST integrated moisture flux and its divergence. From the figure, it can be seen that enhanced moisture flux from the tropical regions is directed into Mozambique, South Africa, and Zimbabwe. This results in a positive bias in moisture convergence and precipitation (Fig. 3b). The bias in the WRFPWP moisture forecast (Fig. 5f) shows enhanced tropical moisture flux being directed toward Madagascar. The moisture flux from the southwestern Indian Ocean into the southern Africa landmass is slightly enhanced and is seen increasing the moisture convergence over the central Mozambique region. The moisture flux biases in the WRF model coupled to a simple mixed layer ocean model forecast are less, relative to the moisture flux biases in the WRFSSST forecast, resulting in an improved spatial distribution of precipitation over southern Africa.

d. Sea surface temperature and surface air temperature over land

The SST estimated by OISST2 during DJF 2011/12 (Fig. 6a) shows a region of high temperature (>28°C) over the tropical South Indian Ocean. The SST across the east coast of southern Africa during DJF 2011/12 varies from about 22° to 28°C from the tropics to the subtropics. The west coast of southern Africa is cooler at about 18°C. The SINTEX-F forecasted SST (Fig. 6b), which was used as a lower boundary in the WRFSSST forecast, shows significant warm temperature biases of more than 0.5°C over the Mozambique Channel and along the east coast of southern Africa with a maximum bias of 2°C over the Agulhas region (Fig. 6b). Significant negative biases are seen over the rest of the South Indian Ocean with up to a 2°C cool bias in the tropical South Indian Ocean (Fig. 6b). Most regions of the South Atlantic show positive biases, except to the west of the South African coast (Fig. 6b). Interestingly, the ensemble mean of the PWP mixed layer ocean model simulated SST (Fig. 6c) has less of a bias in the tropical Indian Ocean and along the east coast of southern Africa than the SINTEX-F forecasted SST. The PWP model simulated SST shows a slight negative bias of about 0.5°–1°C along the east coast of South Africa. South Atlantic SSTs have biases of about 2°C in the WRFPWP forecast (Fig. 6c), similar to the SINTEX-F forecasted SST. The biases in the SST used in the WRFSSST experiment (Fig. 6b) explain the biases in the forecasted precipitation (Fig. 3b) over the oceanic region. The region of negative bias in SST in the tropical South Indian Ocean region (Fig. 6b) corresponds to the region of negative precipitation bias (Fig. 3b), and the region of high SST bias along the east coast of southern Africa (Fig. 6b) enhances the moisture and hence the positive precipitation bias over the ocean along the coast of southern Africa (Fig. 3b). The PWP model, which forecasted higher SST over parts of the Mozambique Channel and over regions around Madagascar, results in a higher precipitation bias (Fig. 3c). However, a slight negative bias in SST of about 0.25°–0.5°C along the coast of southern Africa results in decreasing biases in precipitation relative to WRFSSST forecasts. Warmer SST biases in the South Atlantic result in positive biases in precipitation in both the WRFSSST and WRFPWP forecasts.

The surface temperature over land estimated by GHCN–CAMS shows temperatures above 27°C over the southern

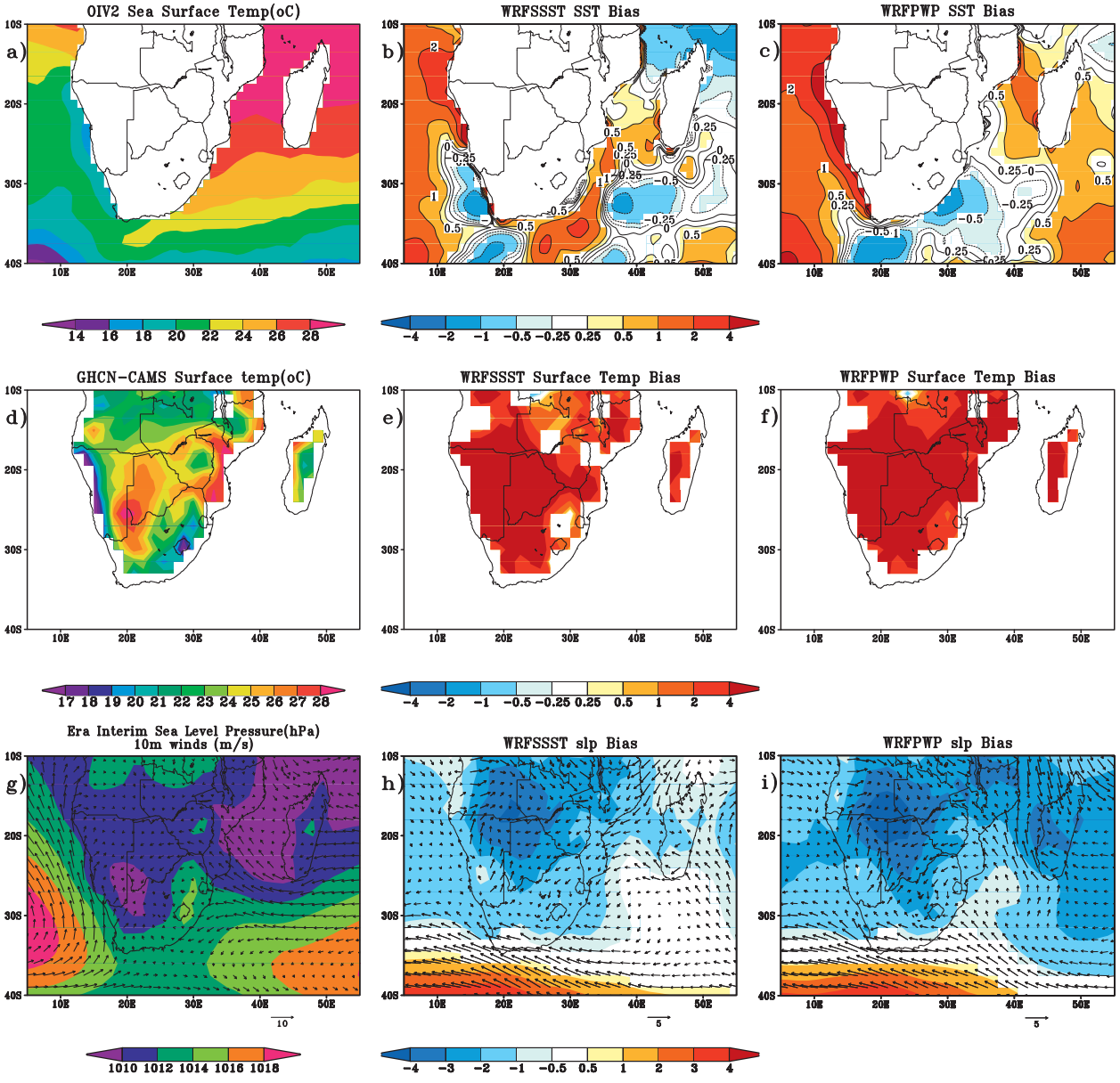

FIG. 6. (a) The OISST2 estimated SST (°C) for DJF 2011/12. (b) Ensemble-mean bias in SST specified to WRF in the WRFSSST experiment (significant at 90% using a Student's *t* test). (c) Significant (at 90% using a Student's *t* test) bias in SST forecasted by WRFPWP. (d) GHCN–CAMS estimated land surface temperature for DJF 2011/12 (°C). (e) Ensemble-mean bias in land surface temperature forecast of WRFSSST (°C). (f) As in (e), but for the forecast of WRFPWP. (g) ERA-Interim estimated mean sea level pressure (hPa; shaded) and 10-m wind ($m\,s^{-1}$; vectors, reference vector provided below panel) for DJF 2011/12. (h) Ensemble mean of WRFSSST forecasted sea level pressure (hPa; shaded) and 10-m winds ($m\,s^{-1}$; vectors, reference vector provided below panel). (i) As in (h), but for the sea level pressure forecasted by WRFPWP.

parts of Namibia and parts of South Africa and Botswana (Fig. 6d) during DJF 2011/12. The high temperature region across southern Africa corresponds to the region of low precipitation. Over the tropical southern Africa where high precipitation was observed during DJF 2011/12 (Fig. 2a), the surface temperatures are around 19°–22°C. The ensemble mean of SINTEX-F forecasted surface temperature (figure not shown) shows a significant warm bias of more than 2°C over western parts of southern Africa corresponding to the region of negative precipitation bias (Fig. 3b) forecasted by SINTEX-F. The air temperature bias in the SINTEX-F forecast has maxima over Angola with temperature biases greater than 4°C. The bias in the WRFSSST

ensemble-mean surface temperature forecast is positive over most parts of southern Africa (Fig. 6c), with biases of greater than 1°C and more than 4°C over regions of Angola, Namibia, and Botswana. The ensemble mean of WRFPWP on the other hand shows a large positive significant bias greater than 2°C over southern Africa (Fig. 6d).

To understand how the SST biases, which are prescribed in WRFSSST and forecasted in WRFPWP, would have affected the spatial distribution of the precipitation over the southern Africa landmass in the WRF forecasts, we plot significant ensemble-mean sea level pressure biases in the WRFSSST and WRFPWP forecasts with respect to ERA-Interim estimates. Sea level pressure biases are superimposed by significant 10-m winds biases also estimated from ERA-Interim data (Figs. 6h,i). During DJF 2011/12, sea level pressure (Fig. 6g) over southern Africa was between 1010 and 1012 hPa, with sea level pressures less than 1010 hPa over the tropical southwestern Indian Ocean. The 10-m winds (Fig. 6g) clearly show the South Atlantic and South Indian Oceans' subtropical high and southeasterly 10-m winds from the subtropical South Indian Ocean high are seen blowing into the southern Africa landmass (Fig. 6g). The sea level pressure biases over the southern Africa landmass (Figs. 6h,i) are negative, in agreement with the high land surface temperatures forecasted by both WRFSSST and WRFPWP. The warm bias in the SST forecast of SINTEX-F in the Mozambique Channel and cool temperatures over the tropical South Indian Ocean result in a positive equatorward pressure gradient bias with lower pressures over Mozambique Channel relative to the tropical regions (Fig. 6h). This leads to northerly winds from tropics into the Mozambique Channel (Fig. 6h). These moist winds, caused by the pressure gradient between the ocean and the southern Africa landmass, enter Mozambique and increase the precipitation there. Moisture entering Mozambique from the tropical region can also be seen in the integrated moisture flux biases in the WRFSSST forecast (Fig. 5e). The gradient in the SINTEX-F forecasted temperature between the SSTs to the south of Madagascar and the coastal regions (Fig. 6b) results in a pressure gradient favoring southeasterly winds into the southern Africa landmass (Fig. 6h). Because of warm SST near the coast, these winds carry moisture into the southern Africa landmass and increase precipitation.

The SSTs forecasted by the PWP model are warmer in the Mozambique Channel and most of the areas to the east of Madagascar with slight negative temperatures to the northeast of Madagascar (Fig. 6c). The mean sea level pressure bias, in agreement with the bias in the forecasted SST, shows a pressure gradient favoring winds poleward from the tropical regions in the South Indian Ocean. The temperature gradient between the forecasted SSTs to the south of Madagascar and the Mozambique Channel result in 10-m winds from the subtropical region into the southern Africa landmass. The large temperature gradient between these two results in stronger winds blowing into the southern Africa landmass.

The above analysis shows that the errors in the SST forecasted by SINTEX-F, which was specified to the WRF model in the WRFSSST experiment, resulted in more moisture being transported into southern Africa from the South Indian Ocean (Fig. 5e) and the tropical regions. This resulted in an increase in precipitation biases over Mozambique, Zimbabwe, and South Africa in the WRFSSST forecast. The SST forecasted by the WRFPWP model, a result of an adjustment of biases between the WRF and PWP models, results in an SST distribution favoring a realistic distribution of moisture flux and hence precipitation over the southern Africa landmass over Mozambique, Zimbabwe, Botswana, and parts of Zambia.

e. Surface heat fluxes

To better understand the biases in surface temperature forecasted by WRFSSST and WRFPWP, we plot the surface downward net heat fluxes as forecasted by the experiments. The ERA-Interim estimated downward net surface heat flux (Fig. 7a) shows negative values (about $-5\,\mathrm{W\,m^{-2}}$) over Angola, Zambia, northern Mozambique, and Madagascar, corresponding to high precipitation over the region (Fig. 2a), and the net surface heat flux is around $5\,\mathrm{W\,m^{-2}}$ over the rest of southern Africa. The SINTEX-F forecasted significant ensemble-mean net downward surface heat flux (Fig. 7b) is positive over the southern Africa landmass with values of around $5\,\mathrm{W\,m^{-2}}$ over the regions of high precipitation (Fig. 2b), showing biases in the forecasted net surface heat flux. The WRFSSST forecasted ensemble-mean significant net downward surface heat flux (Fig. 7c) shows a positive flux higher than $10\,\mathrm{W\,m^{-2}}$ over the whole of the southern Africa landmass and over $100\,\mathrm{W\,m^{-2}}$ over the South Indian Ocean. The WRFPWP experiment (Fig. 7d) forecasted significant ensemble-mean net downward surface heat fluxes are higher than $30\,\mathrm{W\,m^{-2}}$ over Mozambique, Zimbabwe, Botswana, and parts of South Africa and around $10–30\,\mathrm{W\,m^{-2}}$ over Angola, Zambia, and western South Africa. However, the WRFPWP forecasted net downward surface fluxes are comparable with the ERA-Interim estimates over the South Indian Ocean. To analyze the causes of the biases in the net heat flux forecast, the biases in the components of the surface net heat flux are plotted in Fig. 8.

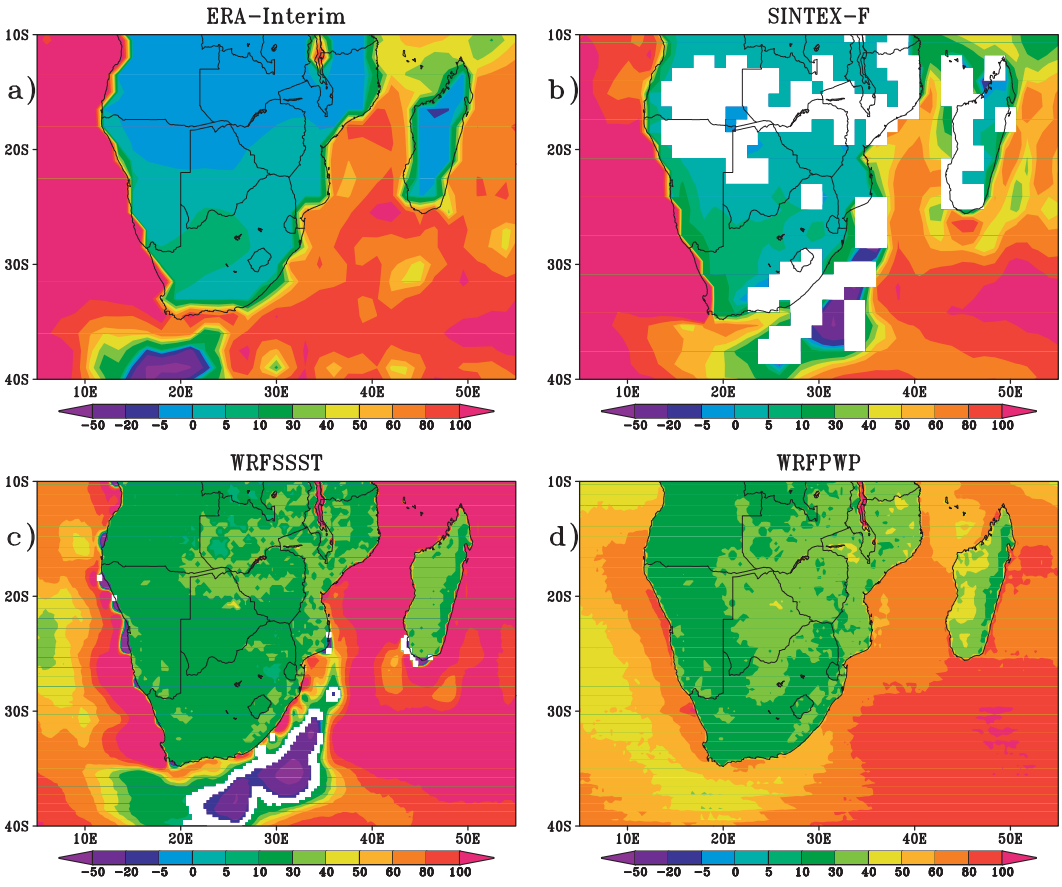

FIG. 7. (a) The ERA-Interim estimated surface net heat flux during DJF 2011/12 ($W m^{-2}$). (b) SINTEX-F forecasted surface net heat flux ($W m^{-2}$) for DJF 2011/12. (c) As in (b), but for the surface net heat flux forecasted by WRFSSST. (d) As in (b), but for the surface net heat flux forecasted by WRFPWP. Surface net heat flux in (b)–(d) is significant at 90% using a Student's *t* test.

The ERA-Interim estimated surface fluxes are shown in Figs. 8a–d. ERA-Interim estimated upward surface latent heat flux (Fig. 8a) shows large values of around 100–120 $W m^{-2}$ over Angola, Mozambique, and Zambia, the region of high precipitation during DJF 2011/12 (Fig. 2a). In agreement with the positive precipitation bias over Zambia, Mozambique, Zimbabwe, and South Africa (Fig. 3b), ensemble-mean WRFSSST forecasted higher significant upward surface latent heat flux (Fig. 8e) over those regions, though significant only over Zambia, Mozambique, and South Africa. The regions of negative and positive upward surface latent heat flux biases in the WRFPWP forecast (Fig. 8i) correspond well with the biases in the precipitation forecasted by the model (Fig. 3c), with negative upward surface latent heat biases over Mozambique, Zimbabwe, Botswana, and Namibia. The upward surface latent heat flux shows higher bias over the tropical South Indian Ocean in the WRFPWP forecast relative to WRFSSST forecast because of a positive bias in precipitation over the region. Because of the two-tier specification of SST in the WRFSSST, large positive SST to the east of South Africa result in a bias of more than 100 $W m^{-2}$ (Fig. 8e) caused by a positive precipitation bias over the region (Fig. 3b). The ERA-Interim estimated net downward surface shortwave radiation flux during DJF 2011/12 shows lower values over the tropical southern Africa landmass (Fig. 8b), corresponding to the high precipitation over the region (Fig. 2a). Cloudiness (figure not shown) caused by high precipitation reduces the downward radiation over the tropical southern Africa landmass and hence the net downward surface solar radiation. Both WRFSSST (Fig. 8f) and WRFPWP (Fig. 8j) show biases of more than 40 $W m^{-2}$ in the net downward surface shortwave radiation over the tropical southern Africa landmass, even though the precipitation distribution shows positive bias in those regions (Figs. 3b,c). The biases in the WRFSSST and WRFPWP downward net surface solar radiation may be caused by an underestimation of cloud cover by the WRF model. Because of the underestimation

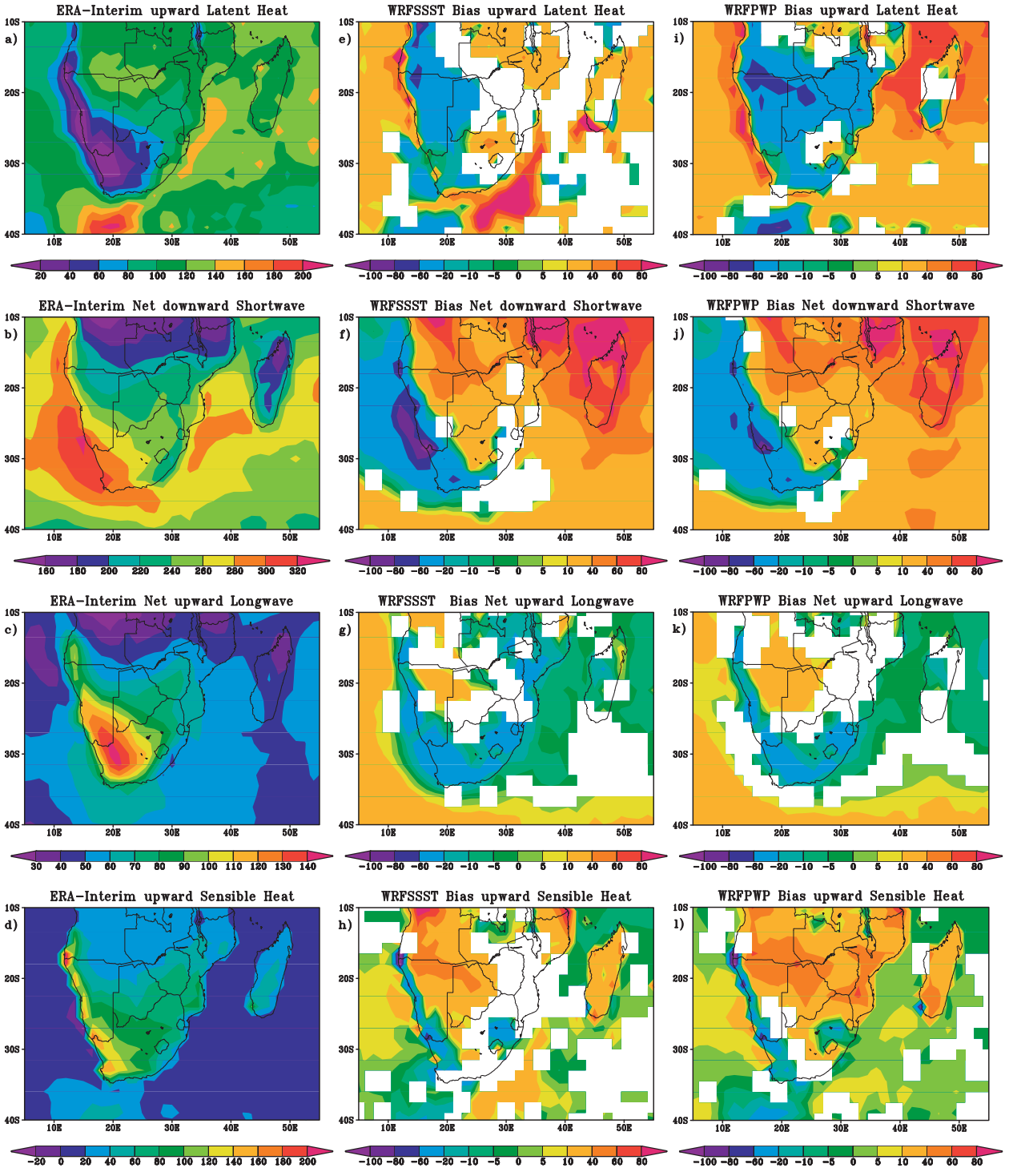

FIG. 8. The ERA-Interim estimated surface (a) upward latent heat flux, (b) downward net shortwave radiation flux, (c) upward longwave radiation flux, and (d) upward sensible heat flux during DJF 2011/12 ($W m^{-2}$). Biases in the WRFSSST forecasted surface (e) latent heat flux, (f) downward net shortwave radiation flux, (g) upward longwave radiation flux, and (h) upward sensible heat flux ($W m^{-2}$). Biases in the WRFPWP forecasted surface (i) upward latent heat flux, (j) downward net shortwave radiation flux, (k) upward net longwave radiation, and (l) upward sensible heat flux. Biases in the fluxes are significant at 90% using a Student's *t* test.

of precipitation over the tropical South Indian Ocean by WRFSSST, the net downward solar radiation shows a large positive bias of above 80 W m^{-2} (Fig. 8f). The WRFPWP also shows a positive bias over the tropical South Indian Ocean (about 60–80 W m^{-2}), though smaller than the WRFSSST forecast. The net upward surface longwave radiation shows values less than 60 W m^{-2} over tropical southern Africa and over the South Indian Ocean in the ERA-Interim estimates (Fig. 8c). Both the WRFSSST (Fig. 8g) and WRFPWP (Fig. 8k) underestimate the upward net surface longwave radiation over most parts of southern Africa, except over parts of Namibia, Botswana, and Angola. The upward net surface longwave radiation is underestimated by about 5–10 W m^{-2} over the South Indian Ocean by both the WRFSSST and WRFPWP forecasts. The ERA-Interim estimated upward surface sensible heat flux during DJF 2011/12 is around 20–40 W m^{-2} over tropical southern Africa and with maximum values of 20 W m^{-2} over the South Indian Ocean (Fig. 8d). The biases in the upward surface sensible heat in the WRFPWP forecast (Fig. 8l) over the southern Africa landmass are higher than those in the WRFSSST forecast (Fig. 8h). The WRFSSST forecasted upward surface sensible heat flux is underestimated by 5–10 W m^{-2} over the tropical South Indian Ocean. However, the WRFPWP forecasted upward surface sensible heat flux is overestimated by about 5 W m^{-2} over the South Indian Ocean, except equatorward of northern Madagascar (Fig. 8l).

The underestimation of the surface upward latent heat flux over the southern Africa landmass roughly equals the overestimation of the upward sensible heat flux in both the WRFSSST and WRFPWP forecasts (Fig. 8). The underestimation of the upward surface longwave radiation is small relative to positive biases in the downward net surface radiation over the southern Africa landmass, showing that the biases caused by the net shortwave radiation, probably because of the underestimation of cloud cover, dominate in the calculation of the total net surface heat flux. The positive biases in the net surface shortwave radiation over the landmass lead to high surface temperatures seen over the southern Africa landmass in forecasts. Over the South Indian Ocean, the biases in the upward surface sensible heat flux roughly equal the upward net surface longwave radiation biases and are of opposite sign and cancel in the calculation of the net surface heat flux in both the WRFSSST and WRFPWP forecasts. The net surface downward shortwave radiation biases in the WRFSSST forecast are higher than the biases in the WRFPWP forecast over the tropical South Indian Ocean mainly because of the lack of air–sea interactions in WRFSSST. The cool bias over the tropical South Indian Ocean in the SST specified to WRFSSST (Fig. 6b) leads to suppression of precipitation (Fig. 3b) and hence the suppression of latent heat flux (Fig. 8e). The suppression of precipitation leads to increase in the net downward solar radiation (Fig. 8f) over the region because of less cloudiness over the region. However, in WRFPWP, the PWP model simulates SST based on the net surface heat fluxes. A larger value of net downward surface radiation results in warmer SST in the PWP model and this in turn increases precipitation and hence increased surface latent heat fluxes over the region. The feedback between the atmosphere and ocean results in an adjustment of the fluxes creating a balance between the fluxes. This adjustment in the fluxes is clearly seen in the upward surface latent heat bias (Fig. 8i) and the net surface downward shortwave flux bias (Fig. 8j) of the WRFPWP forecast over the South Indian Ocean. The increase in precipitation and the latent heat flux caused by the feedback between the WRF and PWP models results in the creation of an area of low pressure over the tropical South Indian Ocean (Fig. 5i) and the low-level winds are seen flowing away from southern Africa.

f. Anomalies forecasted by WRF

As seen from the above analysis, the WRF model forecasted high precipitation and surface temperature over the southern Africa landmass during DJF 2011/12 using SINTEX-F data as boundary conditions. Such biases were also reported in the WRF simulations over a longer period using the reanalysis data (Ratnam et al. 2012), indicating that comparing the forecasts of WRF with respect to its own climate may give a better forecast as is done in most of the general circulation model studies. However, because of the lack of long-term 6-hourly SINTEX-F forecasts an unconventional method is used to generate the mean forecasted climatology of WRF. For generation of the mean forecasted climatology of WRF, we specified the daily-mean long-term climatological SST forecasted by each member from SINTEX-F to WRF and generated an ensemble of WRF forecasts (nine members in total). The daily forecasted SST of SINTEX-F was linearly interpolated to 6 hourly and given as a lower boundary forcing to the WRF model. The SINTEX-F forecast for DJF 2011/12 was used as the initial and lateral boundary condition for these runs. The anomalies for DJF 2011/12 were generated by subtracting each member of the WRF forecasts for DJF 2011/12 from the corresponding member of the WRF with climatological SINTEX-F SST.

The precipitation anomalies forecasted by the WRFSSST with this method (Fig. 9a) are positive over parts of Namibia and Angola and significantly

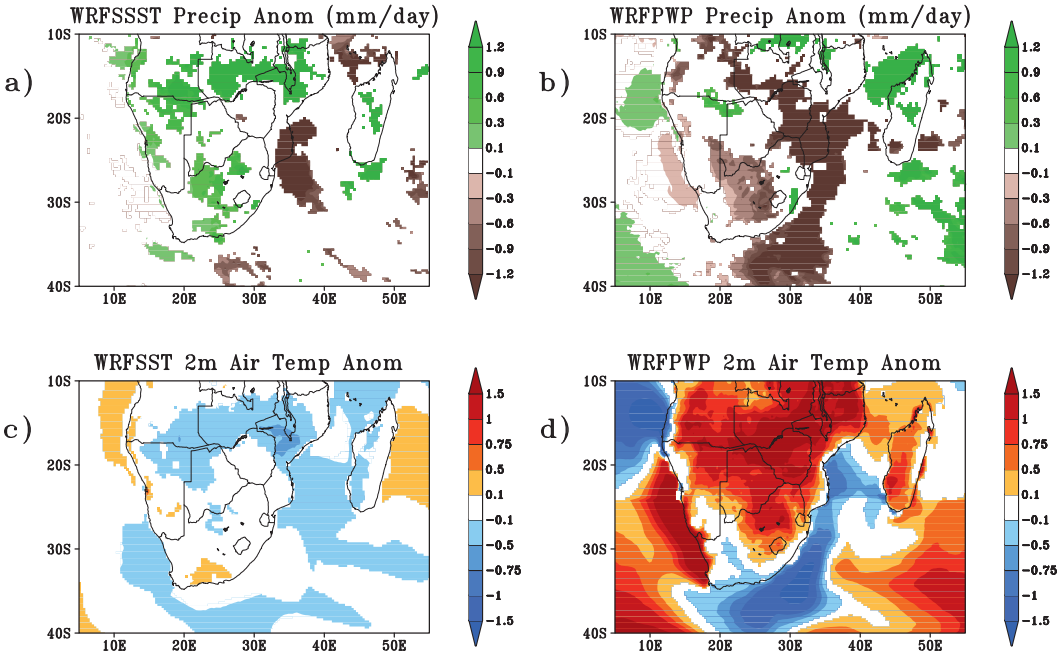

FIG. 9. (a) The WRFSSST forecasted precipitation (mm day^{-1}) significant anomalies during DJF 2011/12. (b) As in (a), but for the precipitation forecasted by WRFPWP. (c) WRFSSST forecasted significant 2-m air temperature (°C) anomalies. (d) As in (c), but for the air temperature forecasted by WRFPWP. The anomalies are significant at 90% using a Student's *t* test.

comparable with the CAMS–OPI estimated precipitation anomalies (Fig. 1c) for DJF 2011/12. However, the WRFSSST forecasted precipitation shows anomalies over South Africa and Zambia to be opposite in phase to the CAMS–OPI estimated anomalies. Interestingly, the WRFPWP forecast (Fig. 9b) for DJF 2011/12 shows negative precipitation anomalies over southern Africa and parts of Mozambique, Zimbabwe, and Zambia, similar to the CAMS–OPI estimated precipitation anomalies. The 2-m air temperature anomalies over land forecasted by WRFSSST (Fig. 9c) for DJF 2011/12 are negative over parts of Namibia, Angola, and Zambia similar to the ERA-Interim estimated anomalies for DJF 2011/12. However, the WRFSST forecasted 2-m air temperature anomalies are opposite in phase to that observed over Mozambique. Over the oceanic regions, the 2-m air temperature anomalies are negative over the Mozambique Channel and near the coast of Mozambique in the WRFSSST simulation (Fig. 6c) similar to the ERA-Interim estimated 2-m air temperatures over the same region. The WRFPWP forecasted 2-m air temperature (Fig. 9d) anomalies show high 2-m temperature anomalies (>1.5) over most parts of southern Africa that are larger than the ERA-Interim estimated 2-m temperatures.

Comparing the WRFSSST and WRFPWP forecasted precipitation in view of the WRF model climatology, the regional downscaling adds value to the SINTEX-F forecasts. For example, the WRFPWP forecasted precipitation anomalies show significant improvements, particularly for the negative anomalies over southern Africa during DJF 2011/12 relative to the SINTEX-F forecasted precipitation anomalies (Fig. 1d). The surface temperatures (i.e., 2-m air temperatures) are generated in the WRF model using a land surface model, which is sensitive to the type of land-use category (Pohl et al. 2011). Hence, more experiments are needed to test the sensitivity of the land surface temperature forecast/simulations in the WRF model to various land surface schemes and also to different land-use categories used in the WRF model.

4. Conclusions

The 3-month lead forecasts of the SINTEX-F coupled general circulation model for DJF 2011/12 was downscaled using the two-tier approach by specifying the SINTEX-F forecasted SST as the lower boundary (the WRFSSST experiment). In addition to this, a one-tier approach of downscaling is also employed by coupling the WRF to a PWP mixed layer ocean model (the WRFPWP experiment). The WRFSST precipitation forecasts show enhancement of precipitation over most parts of southern Africa relative to the SINTEX-F

forecasted precipitation, thus increasing the positive biases in the precipitation forecast. The WRFPWP forecast on the other hand shows a realistic distribution of precipitation during DJF 2011/12. A comparison of the WRFPWP precipitation forecasts with those of SINTEX-F shows a reduction in precipitation biases, thus adding value to the SINTEX-F forecast. The precipitation biases are seen to be related to biases in the vertically integrated moisture fluxes generated by the models. The vertically integrated moisture flux simulated by SINTEX-F shows a region of significant convergence bias corresponding to the regions of high positive precipitation bias over southern Africa during DJF 2011/12. The WRFSSST driven by the SINTEX-F boundaries enhanced the vertically integrated moisture fluxes and created a high positive precipitation region over southern Africa. The WRFPWP, in which air–sea interactions take place because of the exchange of fluxes between the WRF and PWP models, improved the vertically integrated moisture fluxes forecasted relative to the SINTEX-F and WRFSSST.

The SST forecasted by the PWP model for DJF 2011/12 showed less bias over the South Indian Ocean relative to SINTEX-F, suggesting that the improvements seen in the WRFPWP relative to the WRFSSST was because of the consideration of the air–sea interactions in the WRFPWP model. This is brought out clearly when analyzing the surface heat fluxes. However, the biases in surface temperature over the southern Africa landmass forecasted by both the WRFSSST and WRFPWP are quite high because of biases in the surface fluxes. Further experiments, by using different land surface models, are required to improve the 2-m temperature forecasts over southern Africa.

The results of this study suggest that the downscaling of the SINTEX-F forecast using the WRF model coupled to a simple mixed layer ocean model shows promise in seasonal forecasting over southern Africa during the austral summer. However, the results of this study are limited by the lack of long-term WRF climatology based on the SINTEX-F forecasts. This will be addressed in a future work.

Acknowledgments. The authors would like to thank three anonymous reviewers, Dr. Marcus Thatcher, and Dr. Kim C. Nguyen for their constructive comments and suggestions, which helped to substantially improve the quality of this paper. This research was supported by The Japan Science and Technology Agency (JST)/Japan International Cooperation Agency (JICA) through the Science and Technology Research Partnership for Sustainable Development (SATREPS).

REFERENCES

Behera, S. K., and T. Yamagata, 2001: Subtropical SST dipole events in the southern Indian Ocean. *Geophys. Res. Lett.,* **28,** 327–330.

Chen, Y., and J. Dudhia, 2001: Coupling an advanced land-surface/hydrology model with the Penn State–NCAR MM5 modeling system. Part I: Model implementation and sensitivity. *Mon. Wea. Rev.,* **129,** 569–585.

Cook, C., C. J. C. Reason, and B. C. Hewitson, 2004: Wet and dry spells within particularly wet and dry summers in the South African summer rainfall region. *Climate Res.,* **26,** 17–31.

Cook, K. H., 2000: The south Indian convergence zone and interannual rainfall variability over southern Africa. *J. Climate,* **13,** 3789–3804.

——, 2001: A Southern Hemisphere wave response to ENSO with implications for southern African precipitation. *J. Atmos. Sci.,* **58,** 2146–2162.

Crétat, J., C. Macron, B. Pohl, and Y. Richard, 2011a: Quantifying internal variability in a regional climate model: A case study for southern Africa. *Climate Dyn.,* **37,** 1335–1356, doi:10.1007/s00382-011-1021-5.

——, B. Pohl, Y. Richard, and P. Drobinski, 2011b: Uncertainties in simulating regional climate of southern Africa: Sensitivity to physical parameterizations using WRF. *Climate Dyn.,* **38,** 613–634, doi:10.1007/s00382-011-1055-8.

Dee, D. P., and Coauthors, 2011: The ERA-Interim reanalysis: Configuration and performance of the data assimilation system. *Quart. J. Roy. Meteor. Soc.,* **137,** 553–597, doi:10.1002/qj.828.

Dudhia, J., 1989: Numerical study of convection observed during the winter monsoon experiment using a mesoscale two-dimensional model. *J. Atmos. Sci.,* **46,** 3077–3107.

Fan, Y., and H. Van den Dool, 2008: A global monthly land surface air temperature analysis for 1948-present. *J. Geophys. Res.,* **113,** D01103, doi:10.1029/2007JD008470.

Fauchereau, N., B. Pohl, C. J. C. Reason, M. Rouault, and Y. Richard, 2009: Recurrent daily OLR patterns in the southern Africa/southwest Indian Ocean regions, implications for South African rainfall and teleconnections. *Climate Dyn.,* **32,** 575–591.

Giorgi, F., 1990: Simulation of regional climate using a limited area model nested in a general circulation model. *J. Climate,* **3,** 941–963.

——, and L. O. Mearns, 1999: Introduction to special section: Regional climate modeling revisited. *J. Geophys. Res.,* **104,** 6335–6352.

Hansingo, K., and C. J. C. Reason, 2008: Modeling the atmospheric response to SST dipole patterns in the south Indian Ocean with regional climate model. *Meteor. Atmos. Phys.,* **100,** 37–52.

Hirst, A. C., and S. Hastenrath, 1983: Atmosphere-ocean mechanisms of climate anomalies in the Angola-tropical Atlantic sector. *J. Phys. Oceanogr.,* **13,** 1146–1157.

Hong, S. Y., J. Dudhia, and S. H. Chen, 2004: A revised approach to ice microphysical processes for bulk parameterization of cloud and precipitation. *Mon. Wea. Rev.,* **132,** 103–120.

——, Y. Noh, and J. Dudhia, 2006: A new vertical diffusion package with an explicit treatment of entrainment processes. *Mon. Wea. Rev.,* **134,** 2318–2341.

Huffman, G. J., and Coauthors, 2007: The TRMM Multisatellite Precipitation Analysis (TMPA): Quasi-global, multiyear, combined-sensor precipitation estimates at fine scales. *J. Hydrometeor.,* **8,** 38–55.

Janowiak, J. E., and P. Xie, 1999: CAMS_OPI: A global satellite-rain gauge merged product for real-time precipitation monitoring applications. *J. Climate,* **12,** 3335–3342.

Joubert, A. M., and B. C. Hewitson, 1997: Simulating present and future climate changes of southern Africa using general circulation models. *Prog. Phys. Geogr.,* **21,** 51–78.

——, J. J. Katzfey, J. L. McGregor, and K. C. Nguyan, 1999: Simulating midsummer climate over southern Africa using a nested regional climate model. *J. Geophys. Res.,* **104,** 19 015–19 025.

Kain, J. S., 2004: The Kain–Fritsch convective parameterization: An update. *J. Appl. Meteor.,* **54,** 170–181.

Kgatuke, M. M., W. A. Landman, A. Beraki, and M. P. Mbedzi, 2008: The internal variability of the RegCM3 over South Africa. *Int. J. Climatol.,* **28,** 505–520.

Landman, W. A., and A. Beraki, 2012: Multi-model forecast skill for mid-summer rainfall over southern Africa. *Int. J. Climatol.,* **32,** 303–314. doi:10.1002/joc.2273.

——, M. Kgatuke, M. Mbedzi, A. Beraki, A. Bartman, and A. Piesanie, 2009: Performance comparison of some dynamical and empirical downscaling methods for South Africa from a seasonal climate modeling perspective. *Int. J. Climatol.,* **29,** 1535–1549, doi:10.1002/joc.1766.

Luo, J.-J., S. Masson, E. Roeckner, G. Madec, and T. Yamagata, 2005: Reducing climatology bias in an ocean–atmosphere CGCM with improved coupling physics. *J. Climate,* **18,** 2344–2360.

——, ——, S. Behera, and T. Yamagata, 2007: Experimental forecasts of the Indian Ocean dipole using a coupled OAGCM. *J. Climate,* **20,** 2178–2190.

——, ——, ——, and ——, 2008: Extended ENSO predictions using a fully coupled ocean–atmosphere model. *J. Climate,* **21,** 84–93.

MacKellar, N. C., M. A. Tadros, and B. C. Hewitson, 2009: Effects of vegetation map change in MM5 simulations of southern Africa's summer climate. *Int. J. Climatol.,* **29,** 885–898.

Madec, G., P. Delecluse, M. Imbard, and C. Levy, 1998: OPA 8.1 ocean general circulation model reference manual. LODYC/IPSL Tech. Rep. Note 11, 91 pp.

Mason, S. J., and A. M. Joubert, 1997: Simulating changes in extreme rainfall over southern Africa. *Int. J. Climatol.,* **17,** 291–301.

Mesinger, F., 2008: Bias adjusted precipitation threat scores. *Adv. Geosci.,* **16,** 137–142.

——, and T. L. Black, 1992: On the impact on forecast accuracy of the step-mountain (eta) vs. sigma coordinate. *Meteor. Atmos. Phys.,* **50,** 47–60.

Mlawer, E. J., S. J. Taubman, P. D. Brown, M. J. Iacono, and S. A. Clough, 1997: Radiative transfer for inhomogeneous atmospheres: RRTM, a validated correlated-k model for the long wave. *J. Geophys. Res.,* **102,** 16 663–16 682.

Morioka, Y., T. Tozuka, and T. Yamagata, 2011: On the growth and decay if the subtropical dipole mode in the South Atlantic. *J. Climate,* **24,** 5538–5554.

Nicholson, S. E., and J. Kim, 1997: The relationship of the El Niño-Southern Oscillation to African rainfall. *Int. J. Climatol.,* **17,** 117–135.

Nikulin, G., and Coauthors, 2012: Precipitation climatology in an ensemble of CORDEX-Africa regional climate simulations. *J. Climate,* **25,** 6057–6078.

Pohl, B., J. Crétat, and P. Camberlin, 2011: Testing WRF capability in simulating the atmospheric water cycle over equatorial East Africa. *Climate Dyn.,* **37,** 1357–1379.

Price, J. F., R. A. Weller, and R. Pinkel, 1986: Diurnal cycling: Observations and models of the upper ocean response to diurnal heating, cooling, and wind mixing. *J. Geophys. Res.,* **91,** 8411–8427.

Ratnam, J. V., F. Giorgi, A. Kaginalkar, and S. Cozinni, 2009: Simulation of the Indian monsoon using the RegCM3-ROMS regional coupled model. *Climate Dyn.,* **33,** 119–139.

——, S. K. Behera, Y. Masumoto, K. Takahashi, and T. Yamagata, 2012: A simple regional coupled model experiment for summertime climate simulation over southern Africa. *Climate Dyn.,* **39,** 2207–2217, doi:10.1007/s00382-011-1190-2.

Reason, C. J. C., 2001: Subtropical Indian Ocean SST dipole events and southern African rainfall. *Geophys. Res. Lett.,* **28,** 2225–2227.

——, and H. Mulenga, 1999: Relationships between South African rainfall and SST anomalies in the southwest Indian Ocean. *Int. J. Climatol.,* **19,** 1651–1673.

——, and D. Jagadeesha, 2005: A model investigation of the recent ENSO impacts over Southern Africa. *Meteor. Atmos. Phys.,* **89,** 181–205.

——, W. Landman, and W. Tennant, 2006: Seasonal to decadal prediction of southern African climate and its links with variability of the Atlantic Ocean. *Bull. Amer. Meteor. Soc.,* **87,** 941–955.

Reynolds, R. W., N. A. Rayner, T. M. Smith, D. C. Stokes, and W. Wang, 2002: An improved in situ and satellite SST analysis for climate. *J. Climate,* **15,** 1609–1625.

Roeckner, E., and Coauthors, 1996: The atmospheric general circulation model ECHAM-4: Model description and simulation of present-day climate. Max-Planck-Institut fur Meteorologie Rep. 218, 94 pp.

Rouault, M., P. Florenchie, N. Fruchreau, and C. J. C. Reason, 2003a: South east tropical Atlantic warm events and southern African rainfall. *Geophys. Res. Lett.,* **30,** 8009, doi:10.1029/2002GL014840.

——, C. J. C. Reason, J. R. E. Lutheharms, and A. C. M. Bejaars, 2003b: Underestimation of latent and sensible heat fluxes above the Agulhas Current in NCEP and ECMWF analyses. *J. Climate,* **16,** 776–782.

Seo, H., A. J. Miller, and J. O. Roads, 2007: The Scripps Coupled Ocean–Atmosphere Regional (SCOAR) model, with application in the eastern Pacific sector. *J. Climate,* **20,** 381–402.

Skamarock, W. C., J. B. Klemp, J. Dudhia, D. O. Gill, D. M. Barker, and W. Wang, 2005: A description of the Advanced Research WRF version 2. NCAR Tech. Note TN-468+STR, 88 pp.

Sylla, M. B., F. Giorgi, and F. Stordal, 2012: Large-scale origins of rainfall and temperature bias in high resolution simulations over southern Africa. *Climate Res.,* **52,** 193–211.

——, ——, E. Coppola, and L. Mariotti, 2013: Uncertainties in daily rainfall over Africa: Assessment of gridded observation products and evaluation of a regional climate model simulation. *Int. J. Climatol.,* **33,** 1805–1817, doi:10.1002/joc.3551.

Tadross, M. A., W. J. Gutowski, B. C. Hewitson, C. Jack, and M. New, 2006: MM5 simulations of interannual change and the diurnal cycle of southern African regional climate. *Theor. Appl. Climatol.,* **86,** 63–80.

Vigaud, N., Y. Richard, M. Rouault, and N. Fauchereau, 2007: Water vapor transport from the tropical Atlantic and summer rainfall in tropical southern Africa. *Climate Dyn.,* **28,** 113–123.

Xie, S. P., and Coauthors, 2007: A regional ocean–atmosphere model for eastern Pacific climate: Toward reducing tropical biases. *J. Climate,* **20,** 1504–1522.